WASHINGTON UNIVERSITY
DEPARTMENT OF PHYSICS
LABORATORY FOR ULTRASONICS
St. Louis, Missouri 63130

"Physical Interpretation and Development of Ultrasonic Nondestructive Evaluation Techniques Applied to the Quantitative Characterization of Textile Composite Materials"

Semiannual Progress Report: March 15, 1992 - September 14, 1992

NASA Grant Number: NSG-1601

Principal Investigator:

Dr. James G. Miller
Professor of Physics

The NASA Technical Officer for this grant is:

Dr. Joseph S. Heyman
NASA Langley Research Center
Hampton, Virginia

Introduction

The development and implementation of advanced ultrasonic nondestructive evaluation methods applied to the characterization of composite materials requires a better understanding of the physics underlying the interaction of ultrasound with the material. The purpose of this investigation is to identify and characterize the features of complex, three dimensional materials that limit the ability of ultrasound to detect flaws in this broad class of emerging materials. In order to explore the interaction of ultrasound with such complex media, we investigate the characteristics of ultrasonic fields which have propagated through samples with complex geometries and/or internal architecture. We focus on the physics that underlies the detection of flaws in such materials.

Overview/Background

In the initial phase of the study we examine the magnitude and signature of phase cancellation artifact in measurements made with piezoelectric receivers and the capability of these phase-sensitive measurements to detect the presence of specific defect-mimicking inhomogeneities in the presence of background phase distortion. This is investigated experimentally by making through-transmission signal loss measurements of samples fashioned from Lucite®. One of the Lucite® samples is a ribbed plate designed to produce phase distortion in the transmitted field. The width and spacing of the ribs was chosen to be comparable to the characteristic periodicity found in many of the more common woven carbon/epoxy materials. The other Lucite® sample has flat-bottom holes of uniform depth and varying diameters which have been back-filled with different materials in order to provide several levels of acoustic contrast. The back-filled flat-bottom holes are used to model flaws in structural materials. (A more detailed discussion of the samples is given in the following section.) These samples have been C-scanned in through-transmission mode both individually and in combination with one another. Initially, piezoelectric receivers were used and the measured data were analyzed using several methods. In subsequent investigations we propose to use an acoustoelectric receiver to distinguish phase cancellation artifacts from true field effects in the piezoelectric data.[1-8]

In a subsequent phase of the study we propose to extend our investigation to examine the effects of ultrasonic propagation through materials with inherently complex architectures. For this part of the study, layered woven carbon/epoxy samples will be employed. One sample will be a flat and parallel woven sample. The other piece will consist of carbon/epoxy tape with back-filled flat-bottom holes as was done with the Lucite® sample. Again, these samples will be

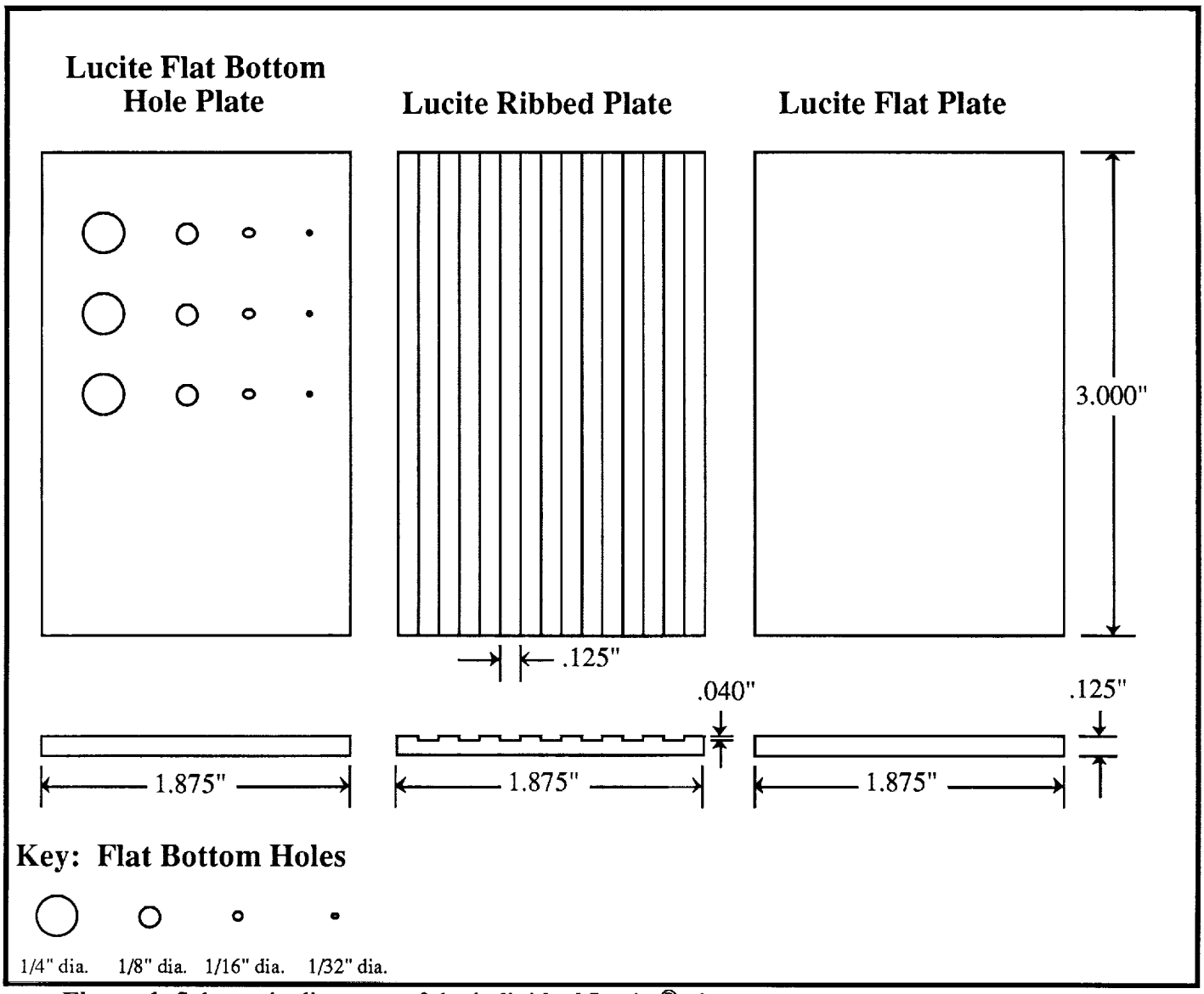

Figure 1. Schematic diagrams of the individual Lucite® pieces.

scanned in the same manner as the Lucite® samples described above. A comparison of the acoustoelectric and piezoelectric data will permit us to understand the potential limitations of piezoelectric measurements for flaw detection in more complex composite structures and allow the development of better inspection methods and strategies. The woven data will also be compared to the Lucite® data to determine whether structures such as the ribbed Lucite® plate are adequate for use in modeling the interaction of ultrasonic fields with woven composite materials.

In this Progress Report, we present the results of the initial phase of the study. We display and discuss data taken from piezoelectric scans using the two Lucite® samples.

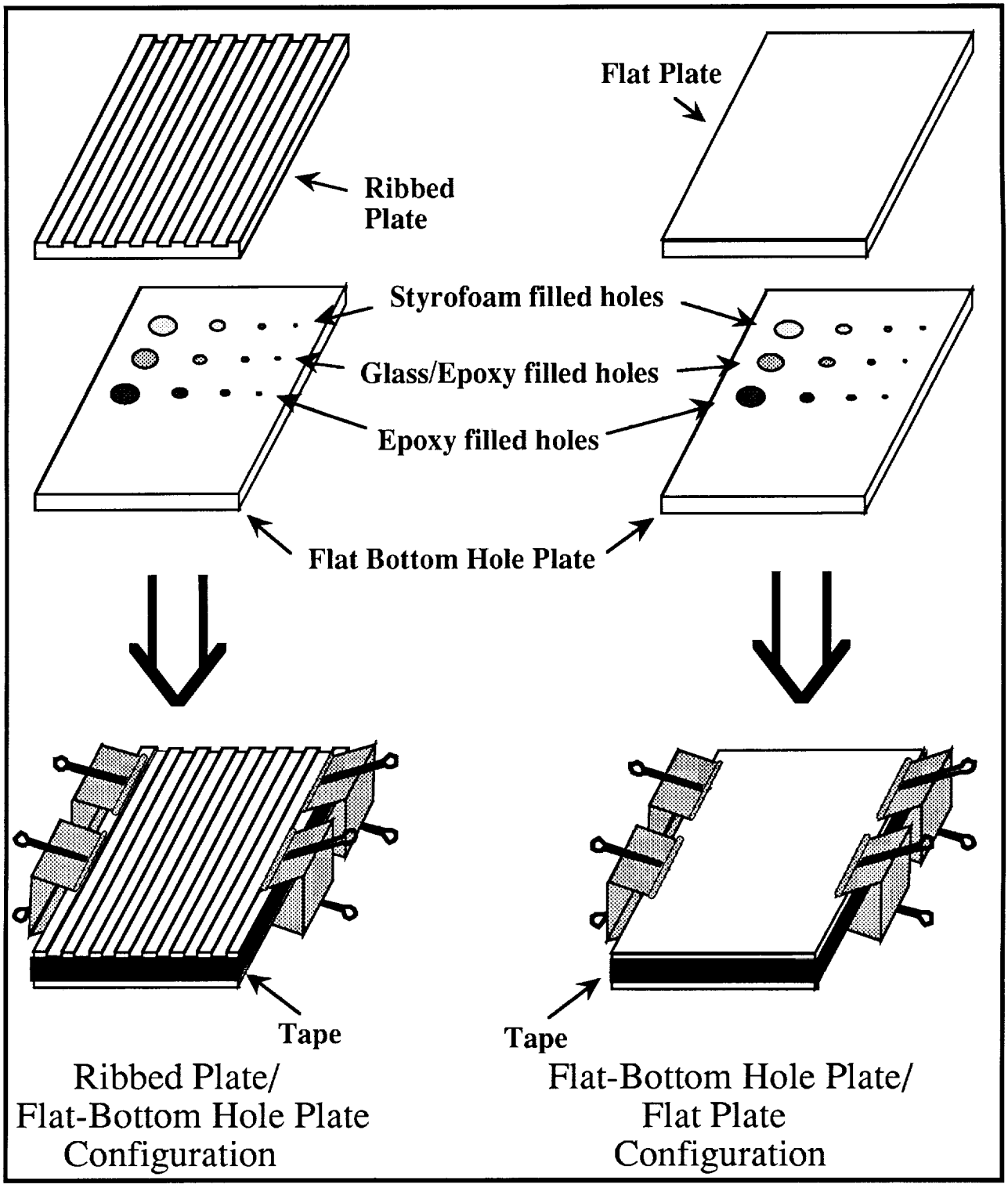

Figure 2. Assembly of the individual Lucite® pieces into the two sample configurations.

Samples/Experimental Set-Up

The samples used in this study were assembled from three constituent pieces, each fabricated from 1/8" thick Lucite®. The first piece was a 3.000" × 1.875" rectangular plate machined with three identical rows of flat-bottom holes. Each row had four holes of varying diameter (1/4", 1/8", 1/16", and 1/32") drilled to a depth of 0.040". The holes in each row were back-filled with different materials: one row of holes was filled with machinable epoxy, one row with a 50/50 mixture (by weight) of epoxy and glass beads (63-158 μm diameter), and one row with styrofoam. After the epoxy-filled rows had cured, the top surface of the Lucite® plate was machined flat so that the back-filled hole surfaces were flush with that of the Lucite®. The second piece used was a ribbed plate which had the same overall dimensions as the flat-bottom hole sample (3.000" × 1.875" × 0.125"). Grooves 1/8" wide and 0.040" deep were machined on one side, parallel to the sample's long axis. These grooves were spaced 1/8" apart. The third piece was a plain flat plate of the same overall dimensions as the other specimens. Figure 1 shows schematic diagrams of the Lucite® pieces.

These three constituents were assembled into the interrogated samples in two different configurations. In one configuration, the ribbed plate was clamped to the flat-bottom hole plate as shown in Figure 2. Sonotech Soundsafe® Industrial Ultrasound Couplant (low viscosity) was placed between the plates before clamping to ensure good acoustic coupling. A narrow strip of tape was placed along the edge of the clamped plates to prevent water from entering into the couplant during immersion. The other configuration used was identical to the one described above except for the substitution of the flat plate for the ribbed plate (see Figure 2).

All measurements in this study were performed in an immersion tank using matched pairs of 0.5" diameter, point-focused (2"), piezoelectric transducers of nominal center frequencies of 5 MHz (Panametrics V309) or 10 MHz (Panametrics V311). The clamped Lucite® sample was positioned such that the interface between the two plates was 2" from the transmitting transducer (i.e. within the focal region). The matched receiving transducer was placed 4" away from the transmitting transducer. For the sample configuration with the flat cover plate with the flat-bottom hole plate, the flat cover plate side was on the transmit side. In the ribbed plate configuration, the ribbed plate was facing the transmitting transducer.

Figure 3 is a schematic diagram showing the data acquisition system used in this investigation. The transmitted ultrasonic signal was a broadband pulse generated by a Metrotek MP215 pulser. The ultrasonic signal obtained from the receiving transducer was first sent

through a pair of step attenuators (HP 355 series) which allowed a more precise adjustment of the signal amplitude to prevent saturation of the electronic equipment. The signal was then sent to a Metrotek MR106 receiving amplifier for further amplification before being sent to a Metrotek MG701 electronic gate. The gate was used to select a 2 μs portion of the signal which included only the first pass of the pulse through the sample. The gated signal was then sent to a HP8557A spectrum analyzer which displayed the power spectrum on a logarithmic scale. An Apple Macintosh II computer was used to read the spectrum and store it for further processing.

The sample consisting of the back-filled flat-bottom holes in combination with the flat cover plate was scanned separately over each row of the holes. The step size (distance between interrogated sites on the sample) of these scans was 0.7 mm in both the x and y directions. The step size was chosen to be slightly less than the diameter of the smallest of the flat-bottom holes. The scans of the ribbed plate/flat-bottom hole plate combination were performed separately over the three rows of holes, also with a 0.7 mm by 0.7 mm step size. Scans of the ribbed plate/flat-bottom hole plate combination were also performed over regions removed from the back-filled holes. In these scans a step size of 0.1 mm was used in both dimensions.

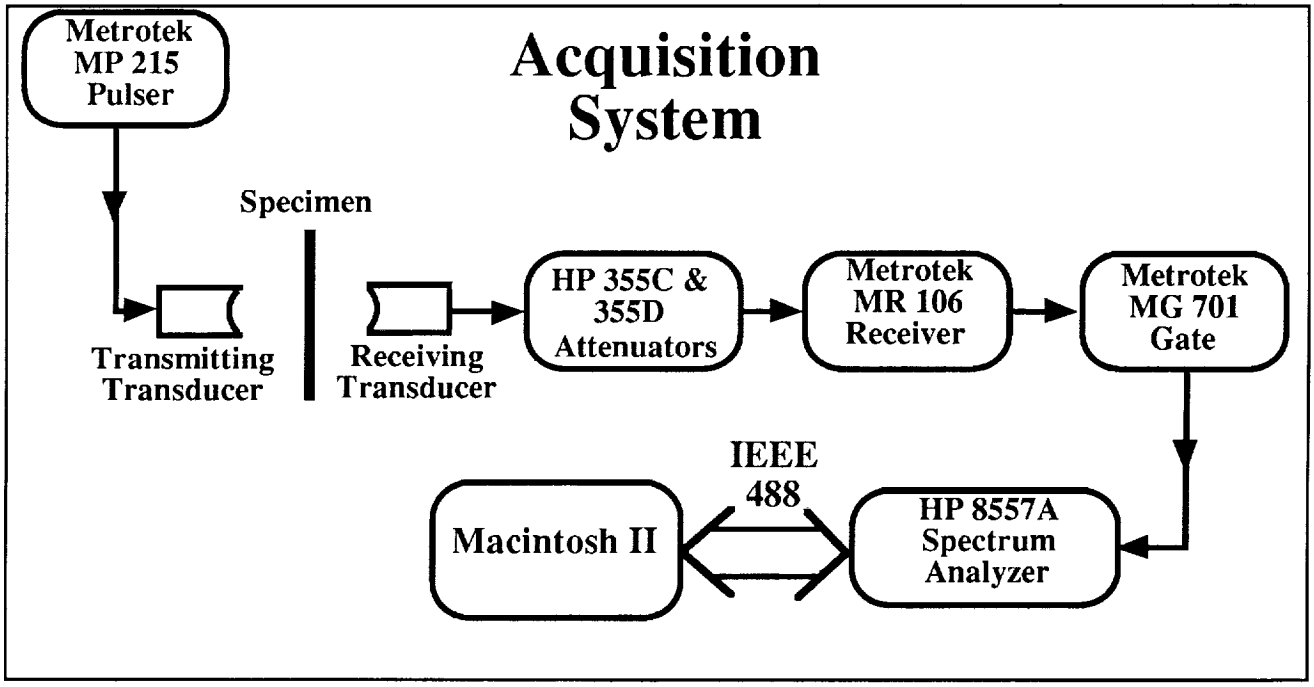

Figure 3. Schematic diagram of the data acquisition system.

Data Analysis

For each interrogated site on a given sample the power spectrum of the received through-transmitted signal was recorded. The power spectra were examined over a broad frequency range and the usable band was determined to be from 2 to 8 MHz. For each data run, a reference power spectrum corresponding to the signal obtained from a water-only path was acquired. The power spectra obtained from the through-transmitted signals (expressed in dBm) was then subtracted from the power spectrum of this reference trace (also in dBm) in the logarithmic domain to deconvolve the response of the equipment from the data. This difference yields a signal loss curve (expressed in dB) as a function of frequency for each interrogated site on the sample. Several analysis techniques were then employed to obtain useful information from the signal loss data.

The first method employed was to average the signal loss over 3 to 7 MHz for each scan site. This was done by converting the signal loss data from dB to the linear domain where the averaging was carried out. The resultant average value was transformed back into dB. The average broadband signal loss values for each site were then collectively displayed as a C-mode image of the scan area.

For further analysis, signal loss data were broken into a succession of narrowband segments, each of 1 MHz bandwidth. Signal loss values in each respective narrowband region were averaged in the linear domain. The resultant average value was then transformed back into dB. This "narrowband" signal loss technique permitted us to examine the frequency behavior of the data in a more detailed fashion than broadband signal loss processing. Displaying the narrowband signal loss information in a C-scan format permitted us to identify those parts of the spectrum in which interesting behavior was occurring. These narrowband images permitted us to identify specific points on the scan where the study of the individual signal loss curves in detail aid in the interpretation of the data.

Results

Three broadband average signal loss images of the flat-bottom hole piece with the flat cover plate are shown in Figure 4. The top image is from the scan of the row of flat-bottom holes back-filled with styrofoam. The middle image is of the row of holes filled with the mixture (50% by weight) of epoxy and glass beads. The final image is from the scan of the holes filled with epoxy only. All three images are mapped to the same grayscale range with white corresponding

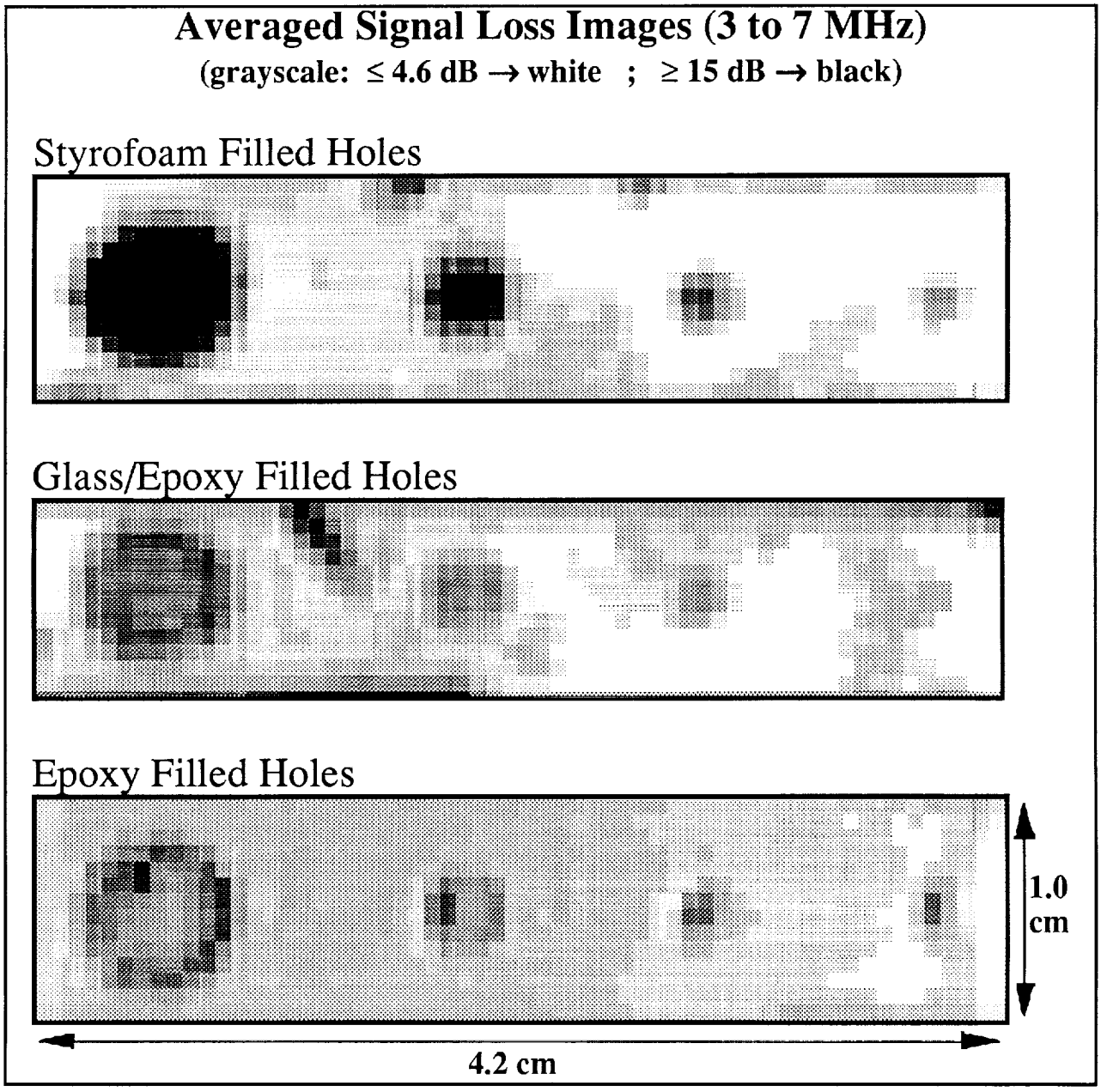

Figure 4. Images from the flat-bottom hole plate/flat plate sample configuration. Each pixel represents 0.7 mm x 0.7 mm on the sample. All images are mapped to the same grayscale.

to 4.6 dB or less of signal loss and black representing 15 dB or more of signal loss. The varying levels of acoustic contrast among the different fill materials are seen. The styrofoam-filled holes display the highest degree of signal loss among the three rows. This is to be expected because styrofoam consists primarily of air bubbles which have an acoustic impedance very different from that of Lucite®.

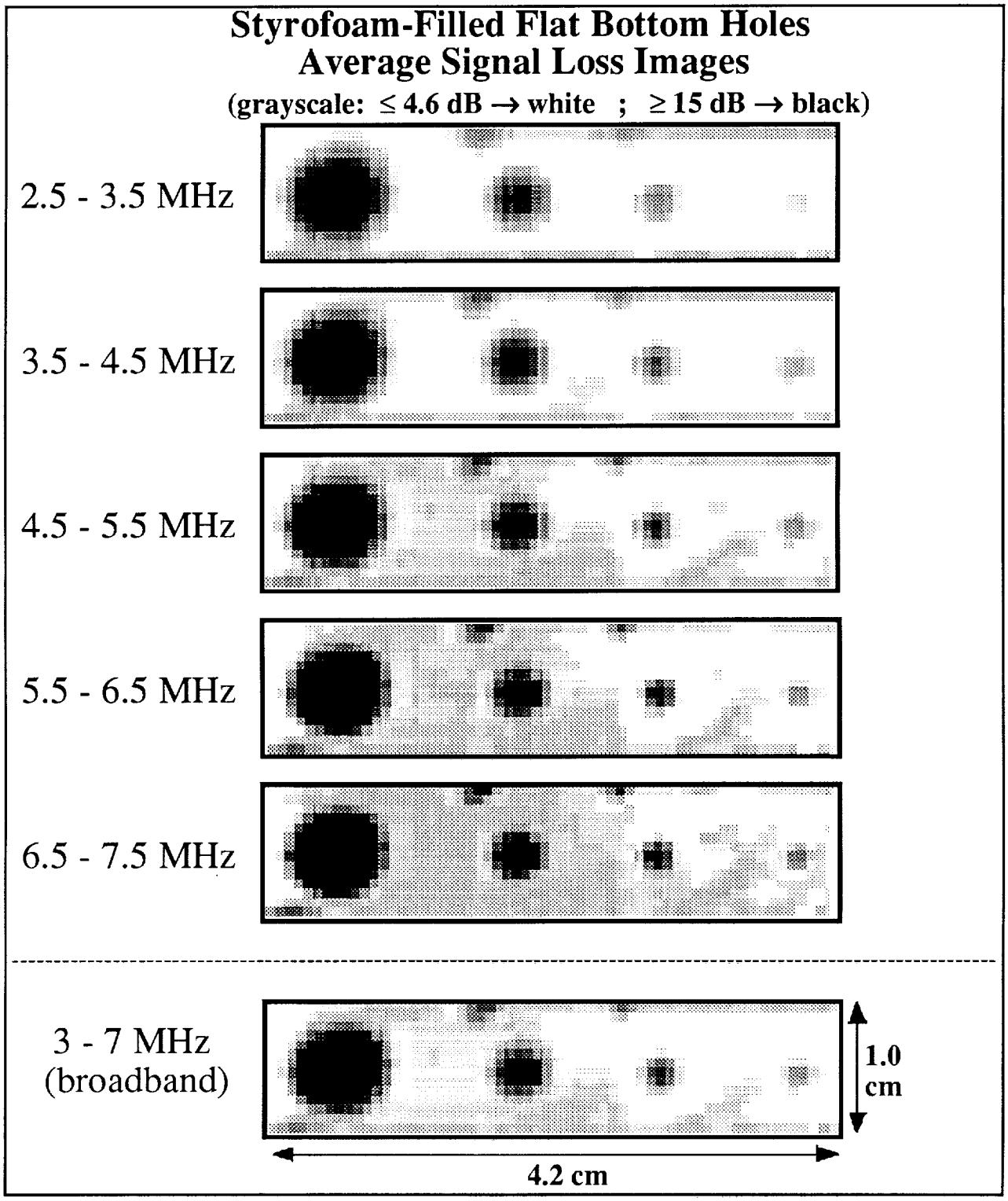

Figure 5. Images of the styrofoam-filled flat-bottom hole region. Each pixel represents 0.7 mm x 0.7 mm on the sample. All images are mapped to the same grayscale.

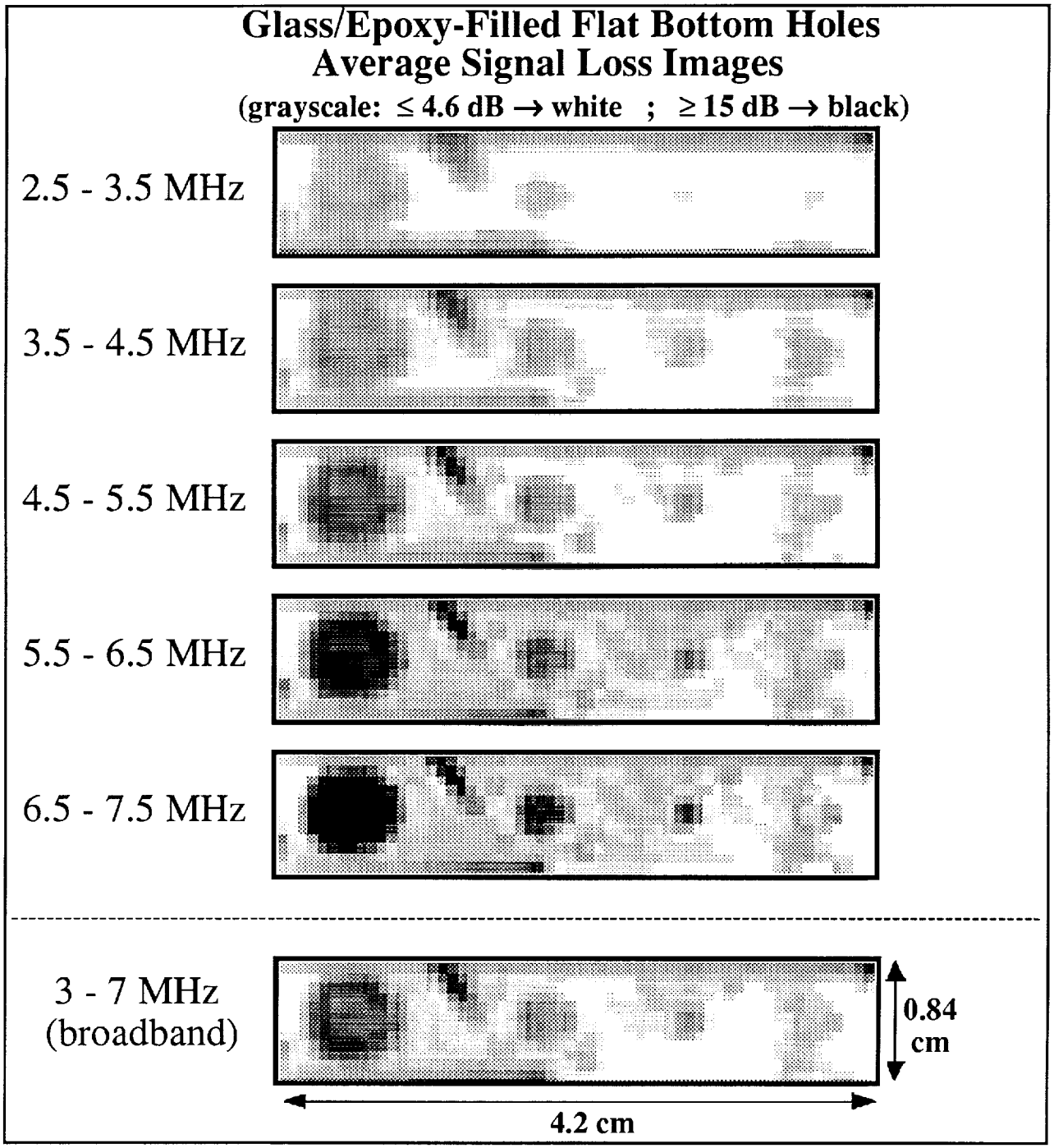

Figure 6. Images of the glass/epoxy-filled flat bottom hole region. Each pixel represents 0.7 mm x 0.7 mm on the sample. All images are mapped to the same grayscale.

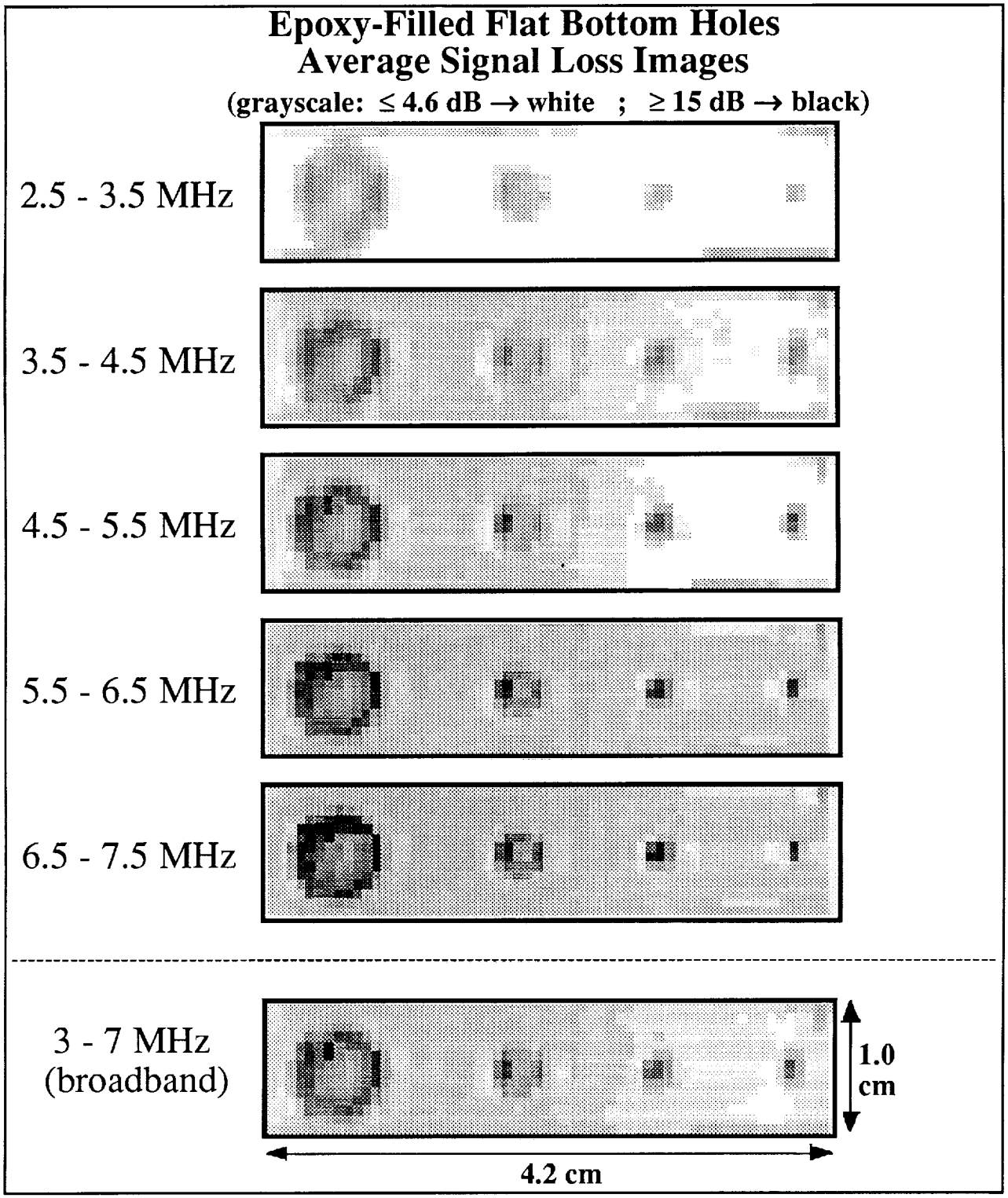

Figure 7. Images over the epoxy-filled flat-bottom hole region. Each pixel represents 0.7 mm x 0.7 mm on the sample. All images are mapped to the same grayscale.

Figure 5 shows signal loss images of the row consisting of the styrofoam-filled flat-bottom holes. The data used to construct these images are the same data used to form the top panel of Figure 4. The top row of Figure 5 is a narrowband-averaged signal loss image of the region. The signal loss was averaged over a 1 MHz wide band centered at 3 MHz. The following four images are the narrowband-average signal loss images centered about 4, 5, 6 and 7 MHz, respectively. The bottom image is the broadband (3 - 7 MHz) average signal loss image included for comparison. All images in the Figure are mapped to the same grayscale, with white corresponding to 4.6 dB or less of signal loss and black signifying 15 dB or more of signal loss. Surveying the narrowband images from the lowest to highest frequency bands, one can see a darkening of the features of the flat-bottom holes. However, each image is qualitatively similar which suggests that the attenuation mechanism responsible for the image features contributes to the signal loss in a similar manner throughout the full bandwidth.

Figure 6 displays narrowband images and a broadband average signal loss image of the row of epoxy/glass-filled flat-bottom holes. The images are displayed in the same format as Figure 5 above. The dark area near the top of the images between the two largest holes is an artifact most likely due to the sample preparation for this particular data run. Among the narrowband images, the features become darker and sharper as frequency increases.

Figure 7 depicts narrowband images and a broadband average signal loss image of the row of epoxy-only filled holes. The images are displayed in the same format as the two previous figures. Again, the features get darker and sharper as one surveys the narrowband images from low to high frequency.

Figure 8 displays three images obtained from the combination flat-bottom hole/ribbed plate sample. The three images are of signal loss averaged over 3-7 MHz. The three images are from the styrofoam row data, epoxy/glass row data, and the epoxy-only row data, respectively. In each of these three images, the two largest flat-bottom holes are still somewhat discernible in spite of the presence of the rib edges of the ribbed plate. However, in all three images, the smallest two holes are quite difficult to identify and locate precisely from the image contrast alone.

Figure 9 shows specific narrowband (1MHz wide) and broadband average signal loss images of the row of styrofoam-filled holes. The first five images are the 1 MHz wide averaged signal loss images centered from 3 to 7 MHz respectively. The bottom image is the broadband 3 to 7 MHz averaged signal loss image included for comparison. The discontinuities in the ribbed

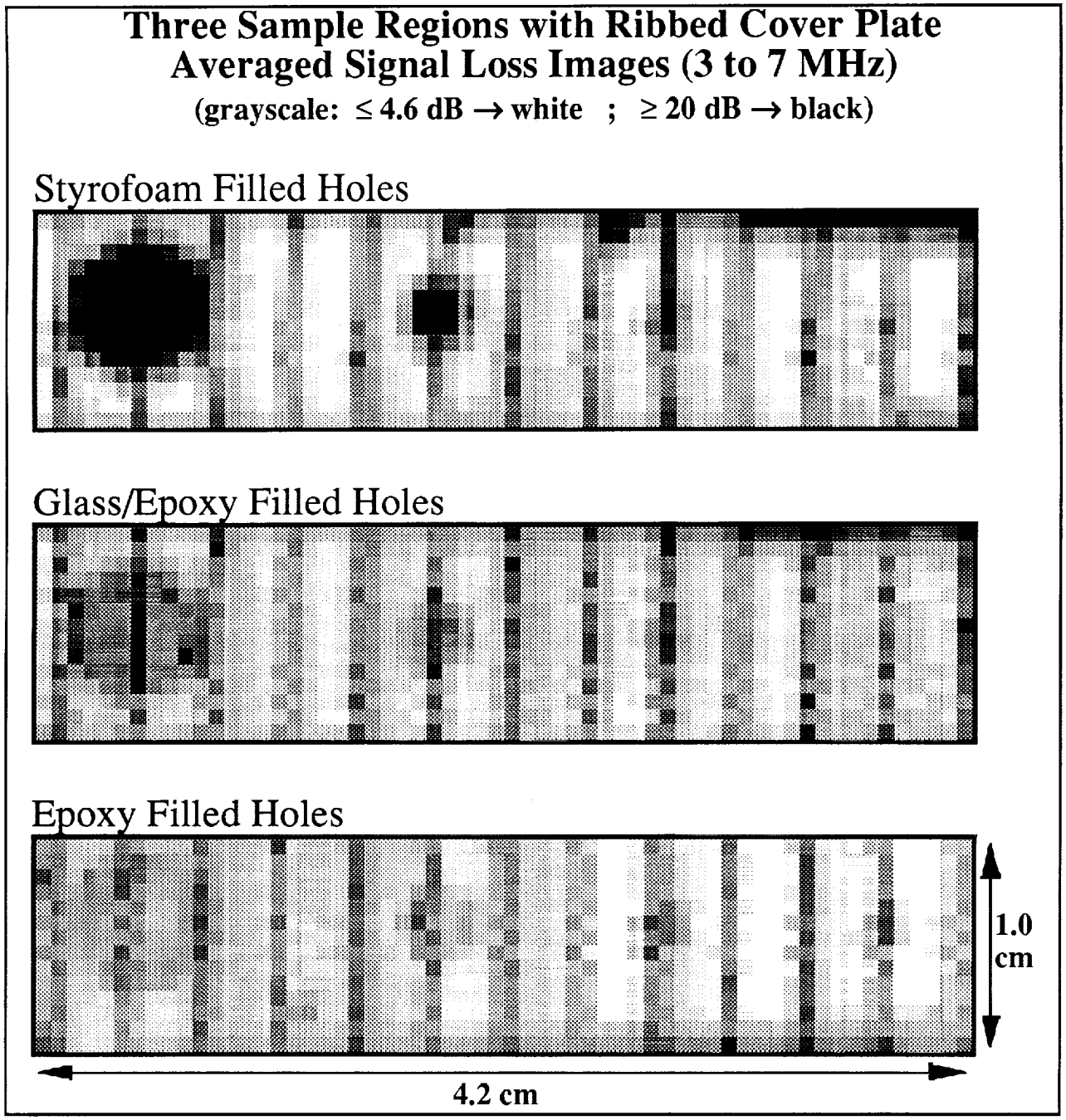

Figure 8. Images from ribbed plate/flat-bottom hole plate sample configuration of the signal loss averaged over 3 to 7 MHz. Each pixel represents 0.7 mm x 0.7 mm on the sample. All images are mapped to the same grayscale.

plate show up in different ways in the images. In the 3 MHz image, only every other rib edge appears at this level of contrast. In the 4 MHz image, the other rib edges appear quite prominently, while those edges occurring in the 3 MHz image are subdued. All of the discontinuities are evident in both the 6 and 7 MHz images and the second smallest hole (third

from the left) is readily identifiable. This same hole can be seen in the 3 MHz image as well. The smallest of the holes can be seen with some clarity in both the 4 and 6 MHz images. In comparing the narrowband images to the broadband image, it can be seen that the narrowband images and the broadband image reveal different features. This seems to indicate that the mechanisms responsible for the rib edge features in the images manifest themselves in different manners and to varying degrees throughout the frequency band.

The images from the glass/epoxy-filled holes with the ribbed plate are shown in Figure 10. The first five images represent the results of averaging the signal loss over a 1 MHz bandwidth centered on each of the integral frequencies from 3 to 7 MHz. Again, the rib edges have a varying degree of presence among the five narrowband images. The 3 MHz image prominently displays one set of rib edges while the 4 MHz image shows the other set. The 6 and 7 MHz images show the second smallest in diameter of the holes. The smallest of the holes shows up rather faintly in the 4 and 6 MHz images.

The images from the epoxy-only holes are displayed in Figure 11. The images are arranged in the same manner as in the previous two figures. The same characteristics (i.e. varying levels of step-discontinuity artifact and flat-bottom hole contrast) present in the images of the other rows are also observed in these images.

Using the ribbed plate/flat-bottom hole plate configuration, we performed a scan over a region removed from the flat-bottom holes in order to study the specific effects of the ribbed plate discontinuities. To enable a more detailed examination of how the phase sensitive detection of ultrasound is affected by the presence of the ribbed plate, the scan was performed using a step size of 0.1 mm by 0.1 mm. Figure 12 shows images obtained from this higher resolution scan. The first five images in Figure 12 represent the narrowband (1 MHz wide) averaged signal loss images from 3 to 7 MHz, respectively. The last image corresponds to the broadband 3 to 7 MHz averaged signal loss image. At the bottom of the Figure are two schematic drawings illustrating how the images correspond with the physical features of the sample. In the 3 MHz image, the leftmost rib edge is readily observable, whereas the rightmost edge is less apparent. This asymmetry in the signal loss between edges is reversed in the 4 MHz image. In each of the respective narrowband images, each rib edge appears with a markedly different degree of contrast.

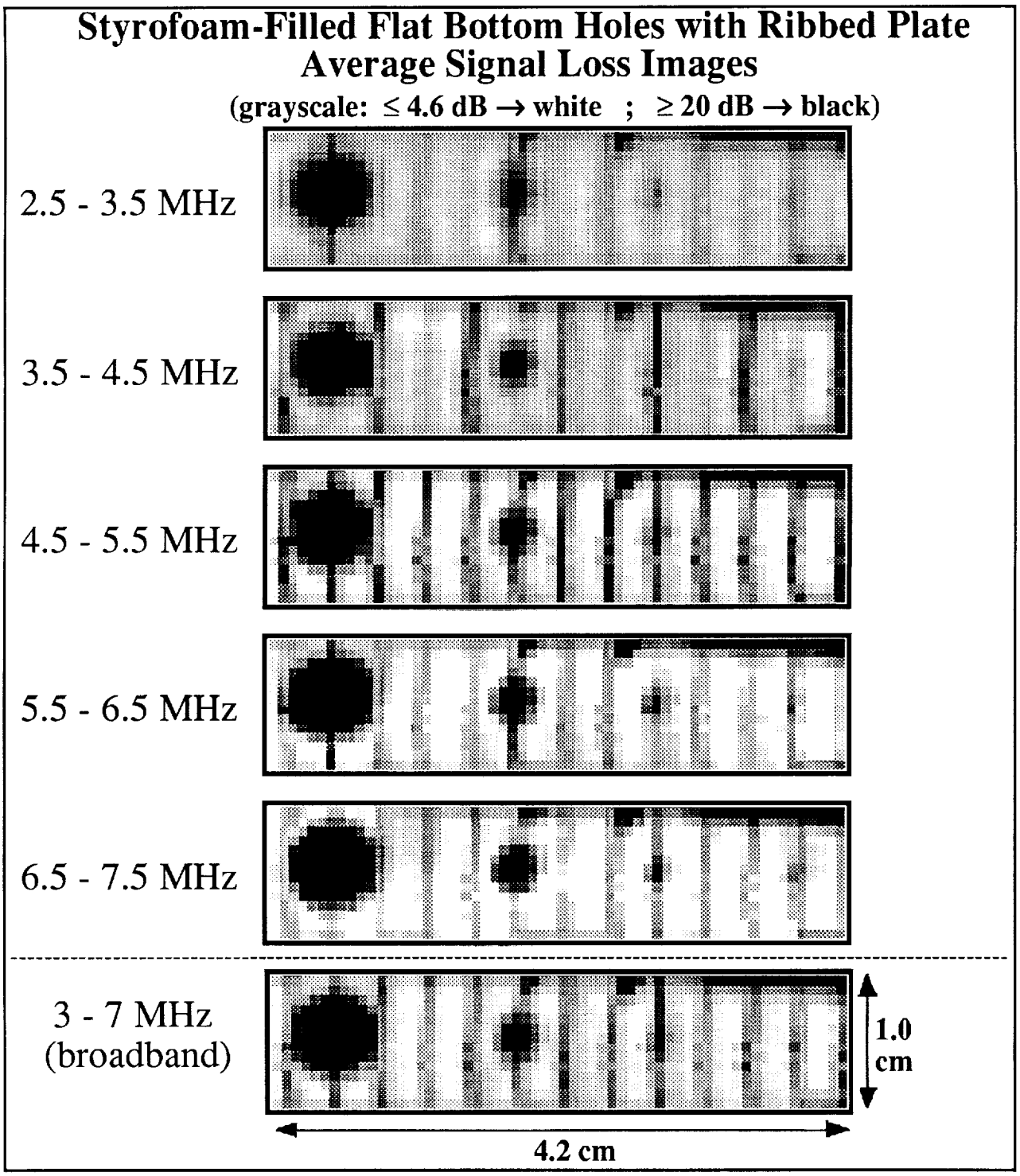

Figure 9. Images of the styrofoam-filled flat-bottom hole region with the ribbed cover plate. Each pixel represents 0.7 mm x 0.7 mm on the sample. All images are mapped to the same grayscale.

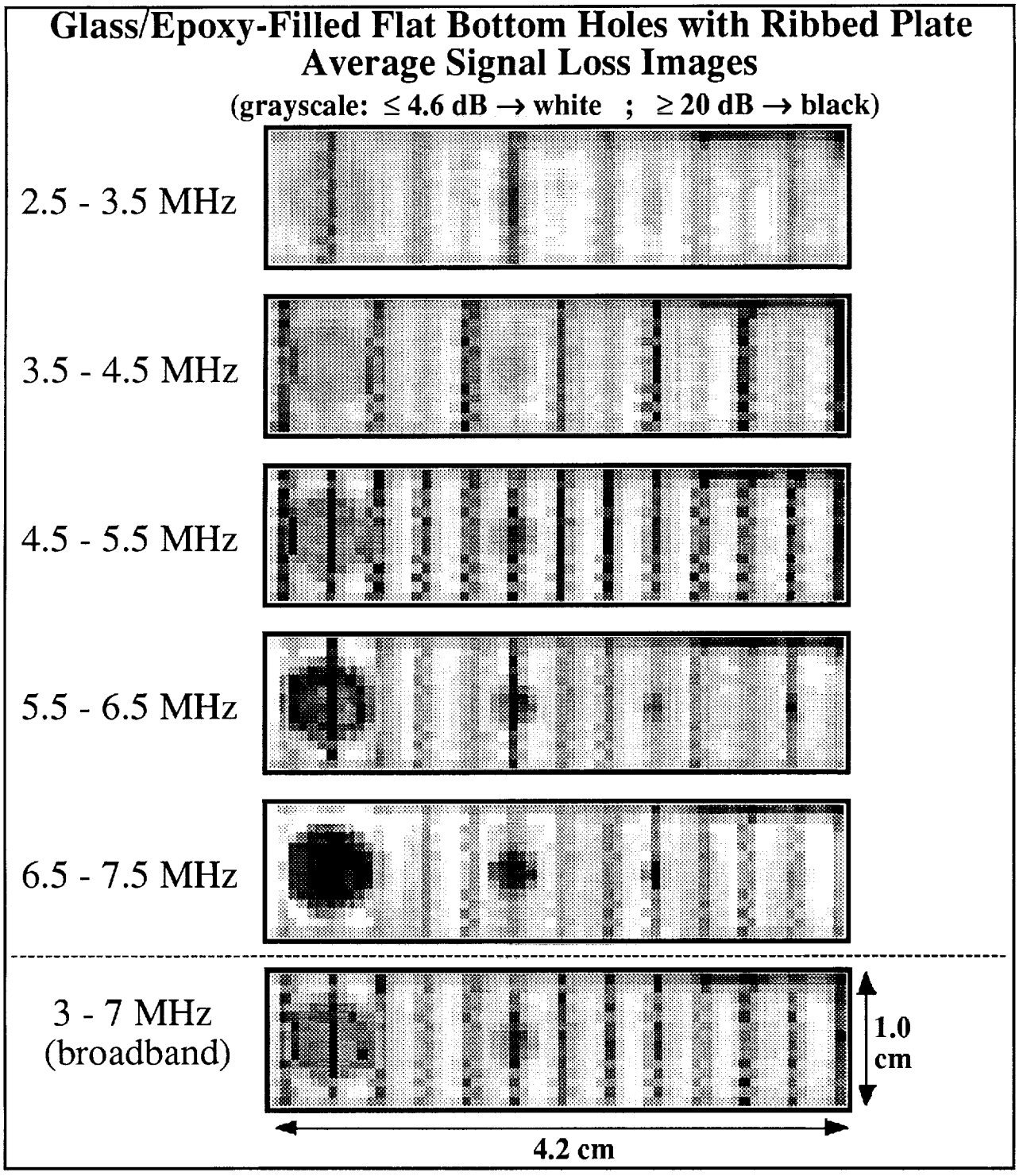

Figure 10. Images of the glass/epoxy-filled flat-bottom hole region with the ribbed cover plate. Each pixel represents 0.7 mm x 0.7 mm on the sample. All images are mapped to the same grayscale.

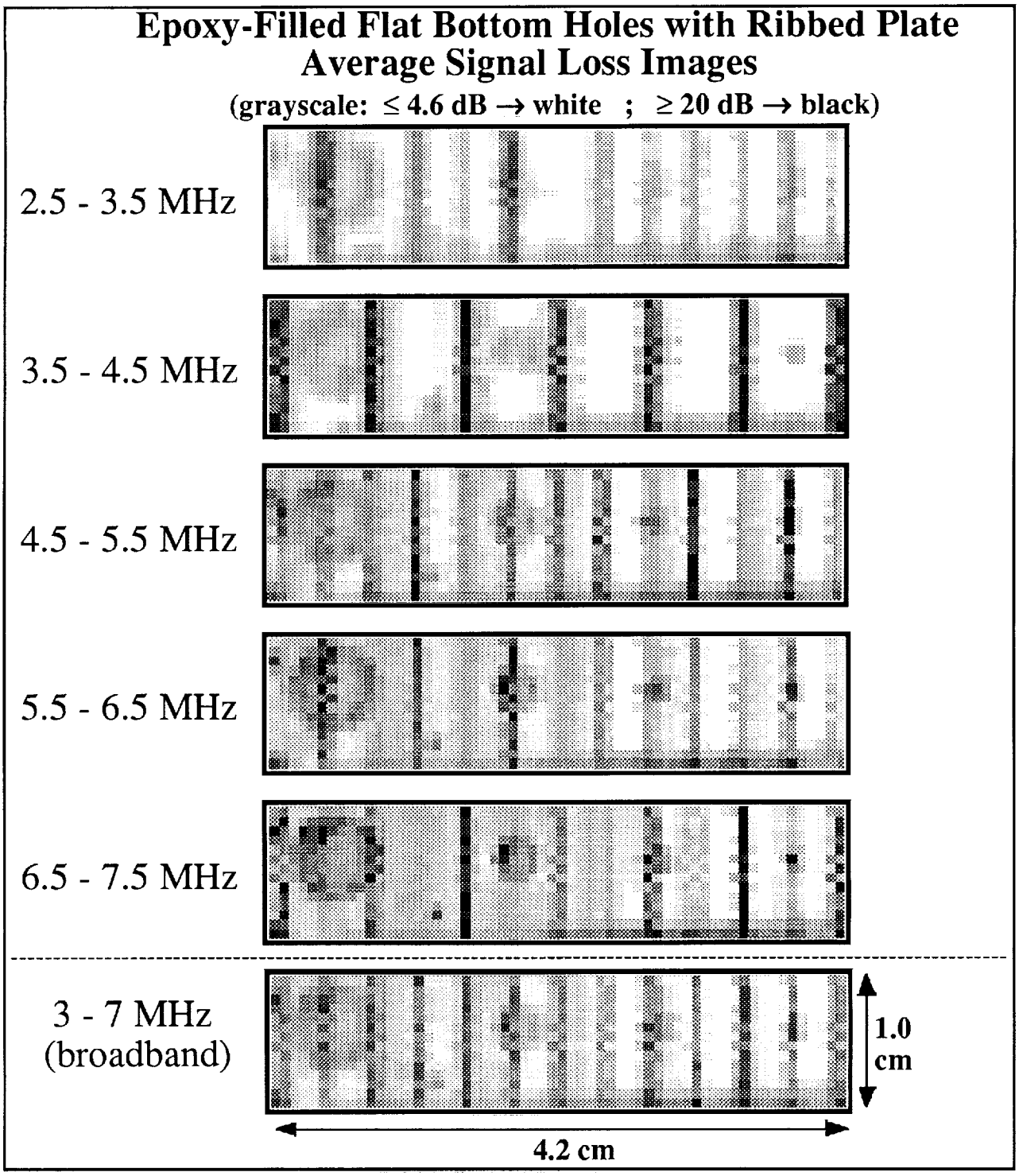

Figure 11. Images of the epoxy-filled flat-bottom hole region with the ribbed cover plate. Each pixel represents 0.7 mm x 0.7 mm on the sample. All images are mapped to the same grayscale.

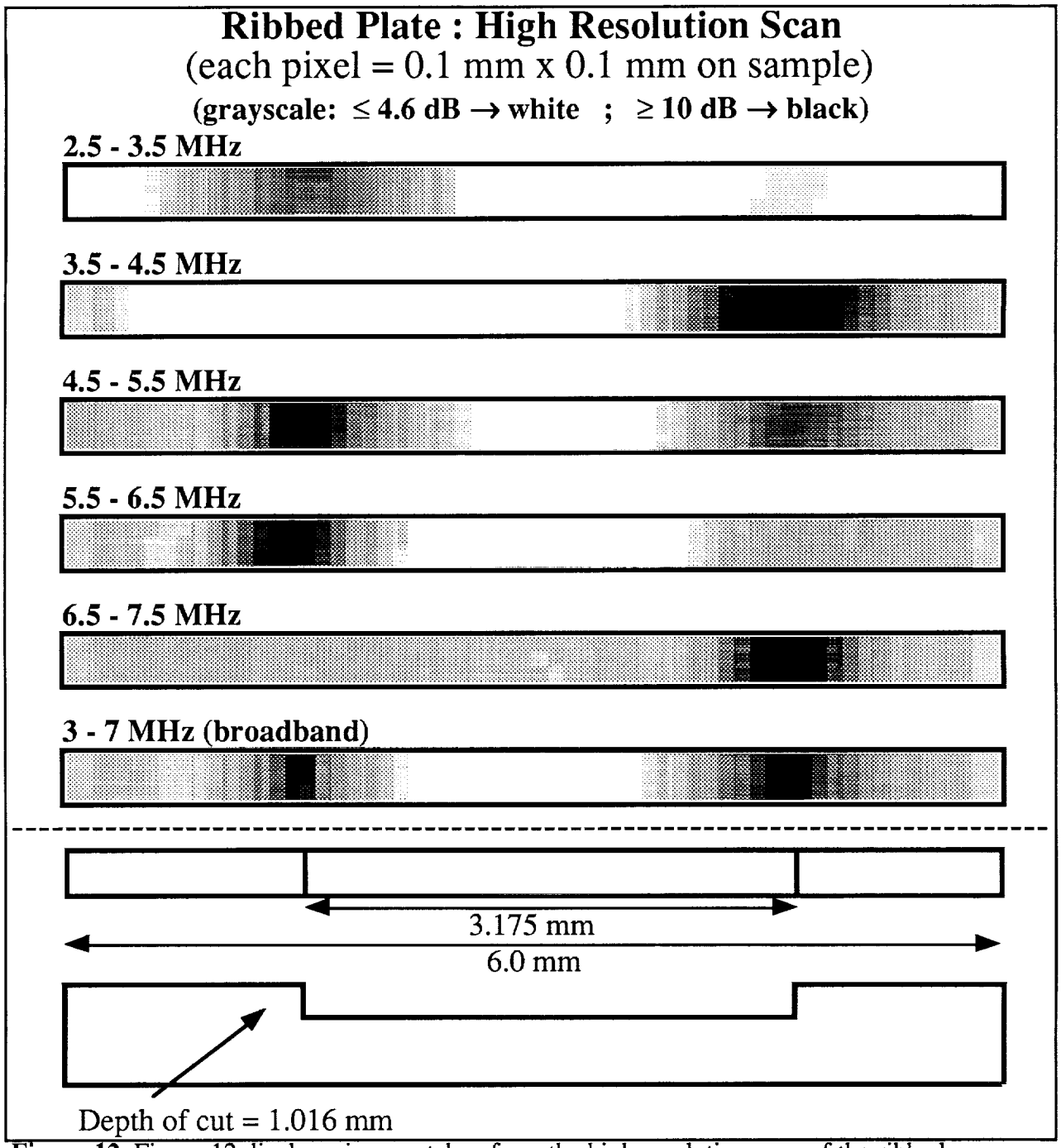

Figure 12. Figure 12 displays images taken from the high resolution scan of the ribbed plate/flat-bottom hole plate sample configuration. The scan was performed over a region of the sample removed from the flat bottom holes in order to investigate the rib discontinuities alone. The top panel is an image of the signal loss averaged over a 1 MHz wide band centered about 3 MHz. The next four panels are images over the same region representing 1 MHz wide signal loss averages centered about 4, 5, 6 and 7 MHz respectively. The last grayscale image is the 3 to 7 MHz wide band averaged signal loss image of the same region. All images are mapped to the same grayscale. Each pixel represents a 0.1 mm x 0.1 mm area on the sample. The two bottom diagrams display the physical characteristics of the sample over the region.

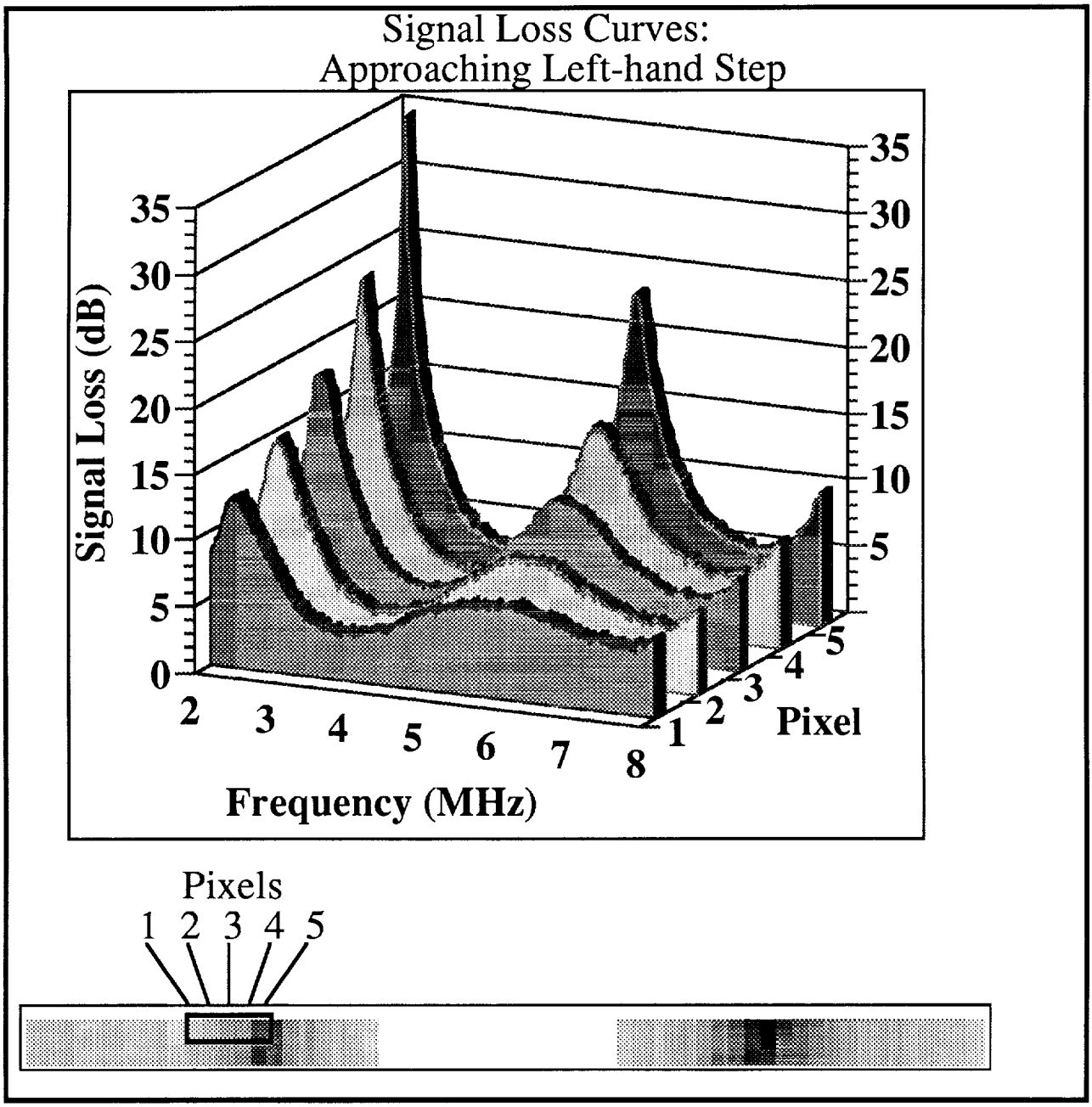

Figure 13. Signal loss traces from five successive scan points from the region shown in Figure 12. The traces from front to back represent the signal loss spectra from five consecutive scan point as the leftmost rib edge (as shown in Figure 12) is approached from the left. The pixels in the scan image which correspond to these points are outlined in the grayscale image below the graph.

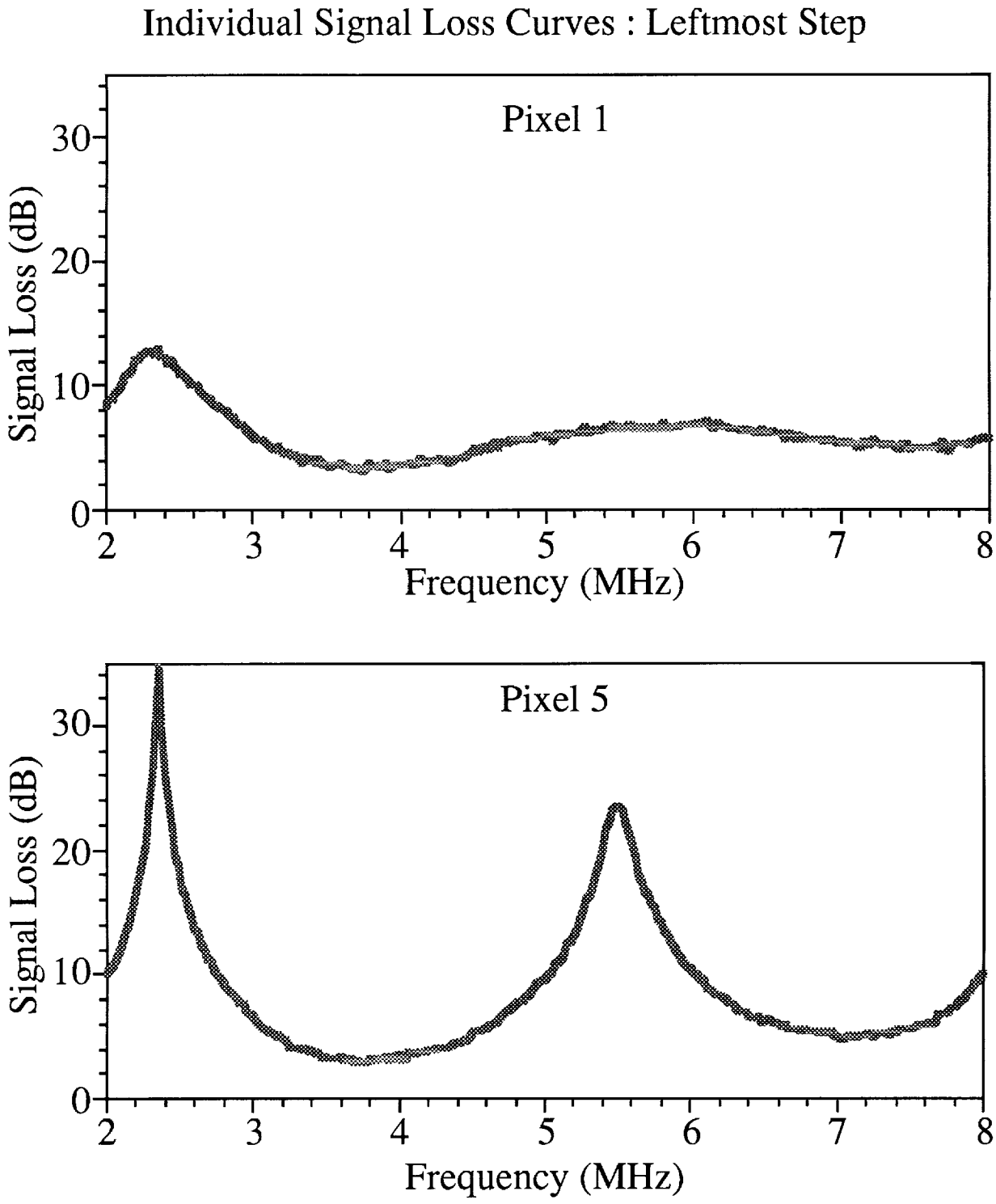

Figure 14. The top graph is a plot of the frontmost signal loss trace from Figure 13. This trace represents the signal loss spectrum from a point approximately 0.4 mm from the leftmost rib edge (as shown in Figure 13). The bottom graph is a plot of the back signal loss trace from Figure 13. This trace represents the signal loss spectrum from a point approximately over the leftmost edge (as shown in Figure 13).

Figures 13 and 14 display the signal loss information from the regions near the leftmost rib edge as shown in Figure 12. Figure 13 depicts the signal loss curves corresponding to five sites from the scan area. Each curve represents the signal loss data obtained from a site on the sample. In turn, these sample points are represented by the individual pixels on the grayscale images. The five pixels outlined in the grayscale image below the signal loss graph represent the scan points from which the displayed signal loss curves were taken. The front-most curve (pixel one) is taken from a point which is approximately 0.4 mm from the rib edge. The rear curve is from a point very nearly on the edge of the rib. Figure 13 highlights some of the qualitative characteristics of the ultrasonic signal loss as the edge is approached. First, there are two regions of large signal loss narrowly distributed about two distinct frequencies. This is the type of behavior one might expect for phase cancellation artifact. Secondly, the low frequency signal loss peak makes itself apparent at a larger distance from the edge than does the high frequency peak. This effect may be due to the larger beam width associated with the lower frequency components of the signal and thus allowing the lower end of the band to "see" the step edge from further away.

Figure 14 shows the signal loss curves from the first and last position of Figure 13 in separate plots. Here it is possible to see in a more quantitative fashion how the signal loss changes as one approaches the step.

Figure 15 displays the signal loss curves as the rightmost step (as illustrated in Figure 12) is approached in the high resolution scan. As in Figure 13, the front-most signal loss trace in the Figure is approximately 0.4 mm from the step edge. Each of the traces are from scan points separated by 0.1 mm. The displayed curves are from the scan points outlined in the grayscale image below the graph. Figure 16 displays the first and fifth signal loss curves from the previous Figure in separate plots. The most significant difference between the signal loss information from the two steps seems to be the change in the frequency location of the signal loss peaks.

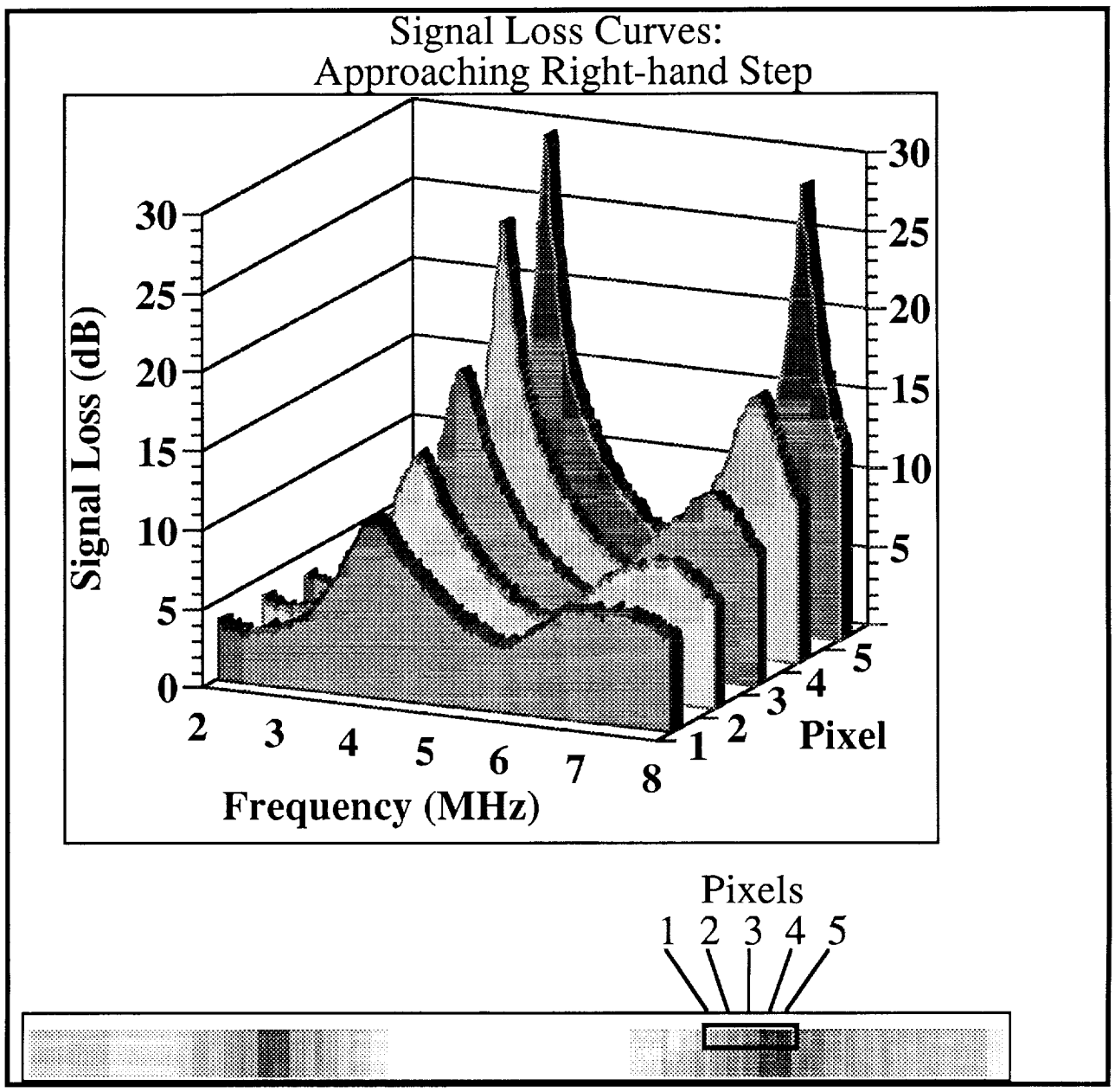

Figure 15. Signal loss traces from five successive scan points from the region shown in Figure 12. The traces from front to back represent the signal loss spectra from five consecutive scan point as the rightmost rib edge (as shown in Figure 12) is approached from the left. The pixels in the scan image which correspond to these points are outlined in the grayscale image below the graph.

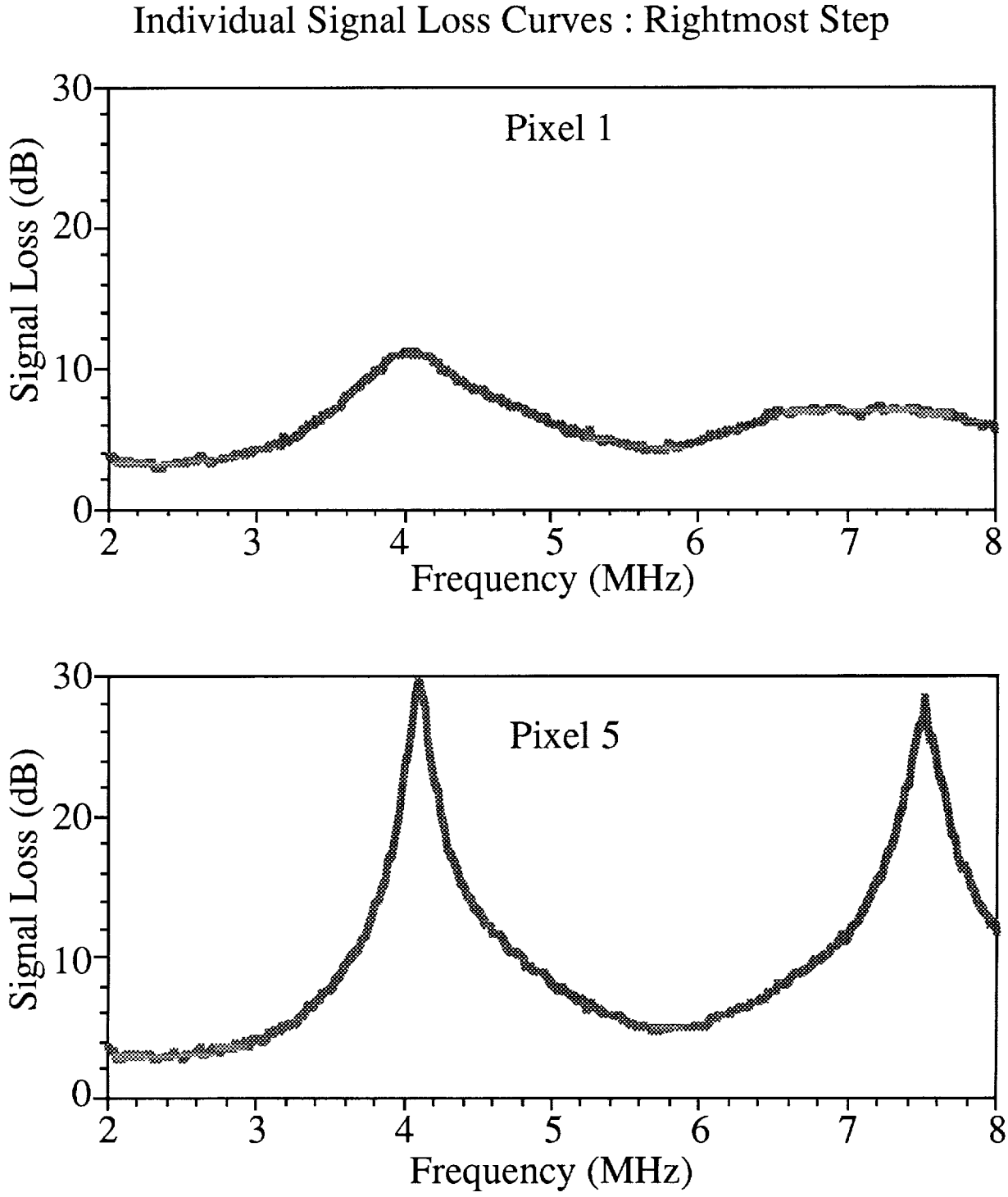

Figure 16. The top graph is a plot of the frontmost signal loss trace from Figure 15. This trace represents the signal loss spectrum from a point approximately 0.4 mm from the rightmost rib edge (as shown in Figure 15). The bottom graph is a plot of the back signal loss trace from Figure 15. This trace represents the signal loss spectrum from a point approximately over the rightmost edge (as shown in Figure 15).

Discussion

From the data shown, it is seen that the signal loss signatures of the discontinuities of the ribbed plate are not located in the same frequency ranges. The right edge of each protrusion causes localized signal loss centered at approximately 2.35 MHz and 5.5 MHz, whereas the left edge of the ribs exhibit signal loss maxima at 4.1 and 7.5 MHz. We hypothesize that the difference in the frequencies is due to some systematic change in dimension that is occurring across the width of the steps on the sample or in the scanning procedure. This change in characteristic length might be caused by thickness changes in the sample systematically induced during preparation. This hypothesis is based upon the fact that the variable frequency signal loss signature of the steps was observed in many independent scans using several different transducers. This seems to suggest that an inherent variation in the thickness across or between the ribs in the ribbed plate may be responsible. However, preliminary measurements using non-ultrasonic means did not reveal any direct indication of a variation in the thickness in the sample that could account for the magnitude of the frequency shift.

The increase in signal loss in the areas near the discontinuities in the ribbed plate are likely to be due to phase cancellation artifact across the face of the receiving transducer. When examining the signal loss values for sites near the steps, the signature of the steps in the signal loss curves are localized in the frequency bandwidth. However, features in the images that are due to acoustic impedance mismatch and/or attenuation contrasts between the bulk and the back-filling materials have signal loss signatures that are more broadband in nature. By avoiding those regions of the band where the phase cancellation artifacts are occurring, the attenuation, impedance mismatch, and scattering mechanisms due to inhomogeneities in the bulk region may be more clearly delineated.[9]

Figure 17 illustrates a case in which selective narrowbanding of the ultrasonic information might aid in flaw detection. The first image in Figure 17 depicts the broadband 3-7 MHz averaged signal loss for the region around the smallest hole back-filled with styrofoam. The second image in Figure 17 displays the same region with the signal loss averaged from 3.25 to 3.75 MHz. In the broadband image, the presence of the flaw cannot be established due the shadowing of the rib edge. However in the second image, the flaw is clearly seen. By knowing the region of the band to avoid, it is possible to identify the signature of the inhomogeneity. Figures 18 and 19 demonstrate the power of this selective narrowbanding approach for images from the smallest glass/epoxy and epoxy-only hole data, respectively.

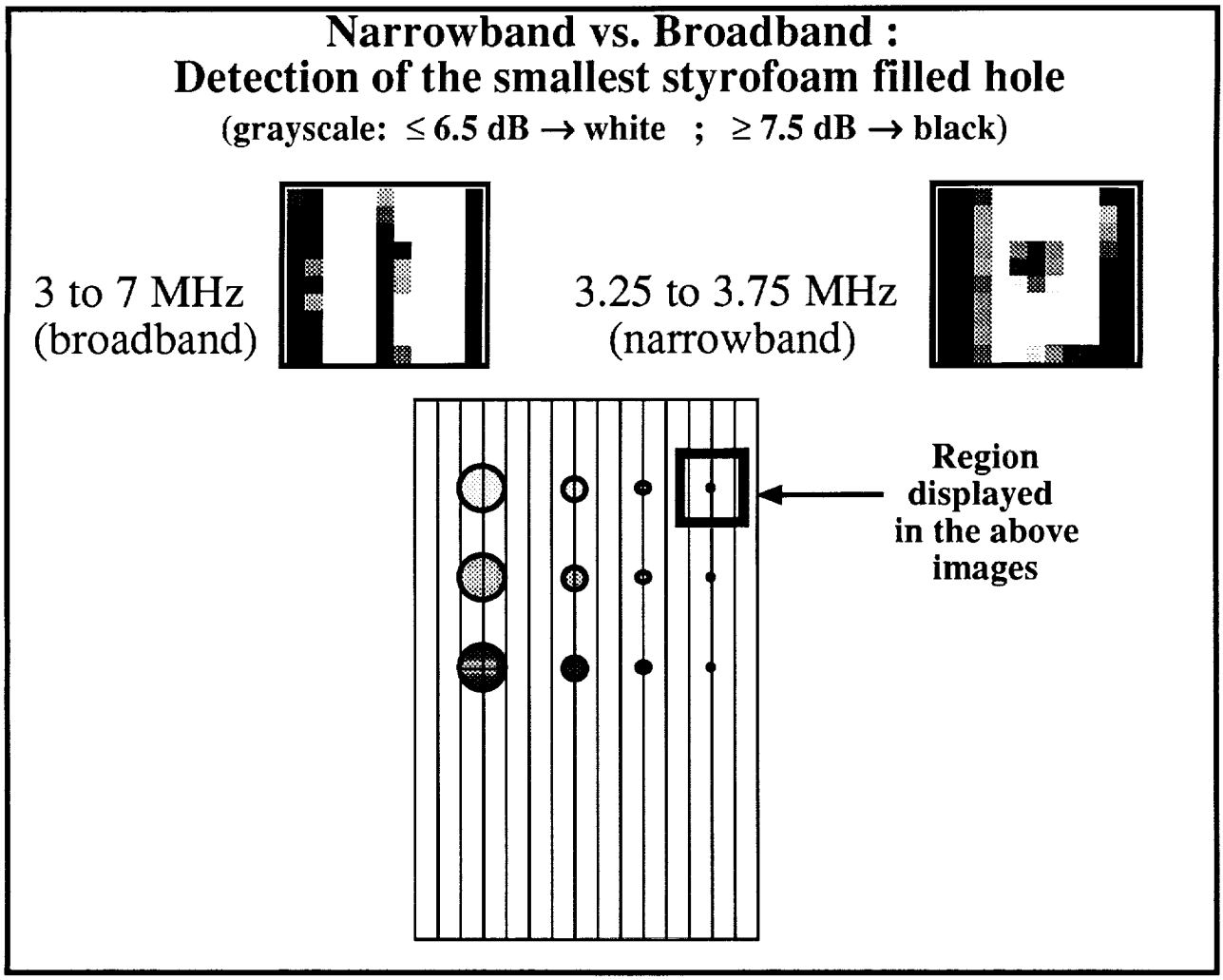

Figure 17. The top left image is of the signal loss averaged from 3 to 7 MHz from the region surrounding the smallest of the styrofoam-filled flat-bottom holes. The top right image is of the signal loss averaged from 3.25 MHz to 3.75 MHz over the same region of the sample. Both images are mapped to the same grayscale with 6.5 dB or less signal loss mapped to white and 7.5 dB or higher signal loss mapped to black. The data used to construct both images is from the scan of the same flat-bottom hole/ribbed plate sample configuration from which the images of Figure 8 and Figure 9 were made. The diagram at the bottom of Figure 17 indicates the portion of the sample to which these images correspond.

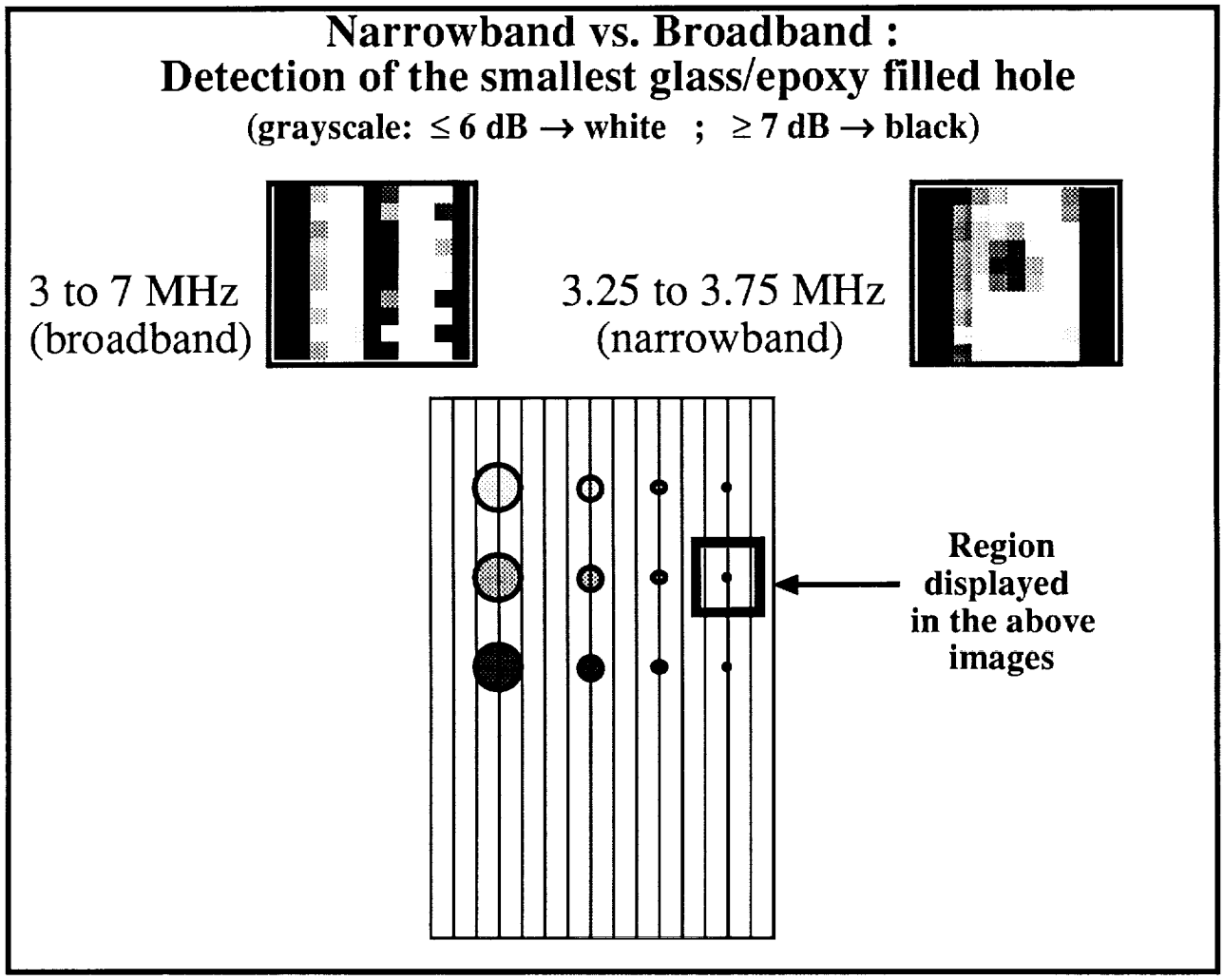

Figure 18. The top left image is of the signal loss averaged from 3 to 7 MHz over the region surrounding the smallest of the glass/epoxy-filled flat bottom holes. The top right image is of the signal loss averaged from 3.25 MHz to 3.75 MHz over the same region of the sample. Both images are mapped to the same grayscale with 6 dB or less signal loss mapped to white and 7 dB or higher signal loss mapped to black. The data used to construct both images is from the scan of the same flat-bottom hole/ribbed plate sample configuration from which the images of Figure 8 and Figure 10 were made. The diagram at the bottom of Figure 18 indicates the portion of the sample to which these images correspond.

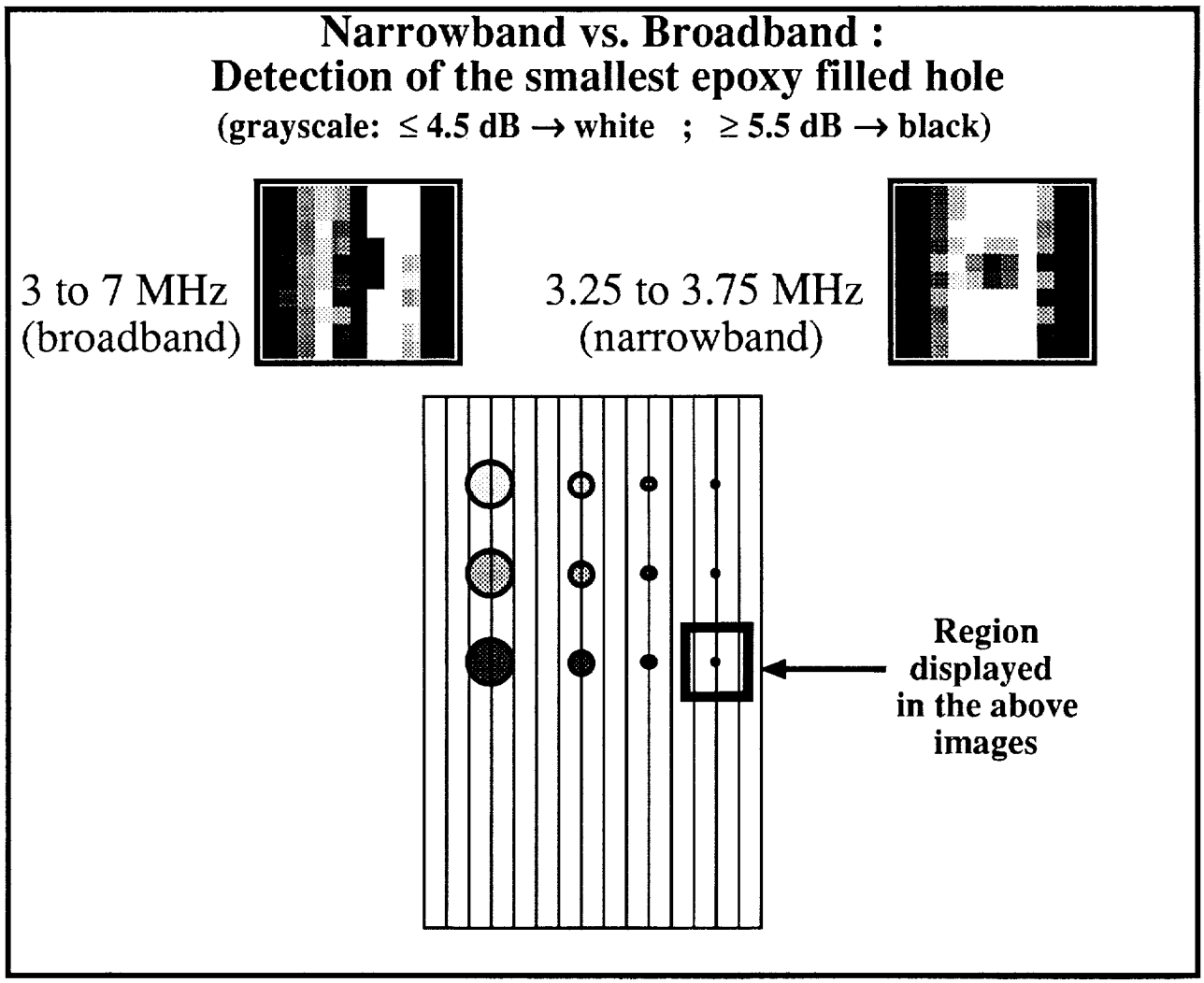

Figure 19. The top left image is of the signal loss averaged from 3 to 7 MHz over the region surrounding the smallest of the glass/epoxy-filled flat-bottom holes. The top right image is of the signal loss averaged from 3.25 MHz to 3.75 MHz over the same region of the sample. Both images are mapped to the same grayscale with 4.5 dB or less signal loss mapped to white and 5.5 dB or higher signal loss mapped to black. The data used to construct both images is from the scan of the same flat-bottom hole/ribbed plate sample configuration from which the images of Figure 8 and Figure 11 were made. The diagram at the bottom of Figure 19 indicates the portion of the sample to which these images correspond.

Woven carbon-epoxy materials may have inherent signal loss characteristics that make flaw detection difficult. If the material distorts the phase of through-transmitted or backscattered ultrasonic fields, then artifacts that would be produced in phase-sensitive receiving apertures may be localized about certain frequencies. These frequency ranges could then be avoided when attempting to quantify inherent bulk properties of the material. The structural nature of the woven materials may cause the occurrence of complex field effects in the through transmitted ultrasound. If there are field effects arising from the periodic nature of the weave pattern or lay-

up, the signal loss signature of these effects may be localized in frequency. Thus, if the material induces phase cancellation artifacts in phase sensitive receivers, or causes dispersion and/or diffraction effects in the field which are localized in frequency, it may be possible to find regions of the band where these effects are minimal and hence broadband absorption and scattering mechanisms are dominant in the measured attenuation. Narrowband averaging of signal loss data in the logarithmic domain (as opposed to the linear domain) may also help contribute to reducing the influence of those features in the spectrum exhibiting large variations over relatively narrow regions of the band and thus enhance the more broadband aspects of the signal loss. This approach may represent a successful strategy for the detection of flaws in woven materials.

References

1. L.J. Busse, J.G. Miller, D.E. Yuhas, J.W. Mimbs, A.N. Weiss, and B.E. Sobel, "Phase Cancellation Effects: A Source of Attenuation Artifact Eliminated by a CdS Acoustoelectric Receiver", *Ultrasound in Medicine*, Vol. 3, pp. 1519-1535, (1977).

2. Mark R. Holland and J.G. Miller, "Phase-Insensitive and Phase-Sensitive Quantitative Imaging of Scattered Ultrasound Using a Two-Dimensional Pseudo-Array", *Proc. IEEE Ultrasonics Symposium*, (1988, Chicago), (Published 1989), Vol. 88 CH 2578-3, pp. 815-819.

3. Joseph S. Heyman and Jr. John H. Cantrell, "Application of an Ultrasonic Phase Insensitive Receiver to Material Measurements"((Published 1977), pp. 124-128.

4. J.S. Heyman, "Phase Insensitive Acoustoelectric Transducers", *J. Acoust. Soc. Am.*, Vol. 64, pp. 243-249, (1978).

5. Patrick H. Johnston and Agus A. Ananda, "The Role of Phase Cancellation in the Ultrasonic NDE of Stitched Graphite-Epoxy Composites", *IEEE Ultrasonics Symposium*, (1991, Orlando, FL), (Proc. IEEE Ultrasonics Symposium, 1991, Published 1992), Vol. 91 CH 3079-1, pp. 845-848.

6. J.R. Klepper, G.H. Brandenburger, L.J. Busse, and J.G. Miller, "Phase Cancellation, Reflection, and Refraction Effects in Quantitative Ultrasonic Attenuation Tomography", *Proc. IEEE Ultrasonics Symposium, Phoenix*, Vol. 77 CH 1264-1SU, pp. 182-188, (1977).

7. J.R. Klepper, G.H. Brandenburger, J.W. Mimbs, B.E. Sobel, and J.G. Miller, "Application of Phase Insensitive Detection and Frequency Dependent Measurements to Computed Ultrasonic Attenuation Tomography", *IEEE Trans. on Biomedical Engineering*, Vol. BME-28, pp. 186-201, (1981).

8. Peter W. Marcus and Edwin L. Carstensen, "Problems with Absorbtion Measurements of Inhomogeneous Solids", *J. Acoust. Soc. Am.*, Vol. 58, pp. 1334-1335, (1975).

9. E. I. Madaras, E. F. Brush, S. L. Bridal, M. R. Holland, and J. G. Miller, "Measured Effects of Surface Cloth Impressions on Polar Backscatter and Comparison with a Reflection Grating Model", *Review of Progress in Quantitative NDE*, (1992, La Jolla, CA), (to be published).